PERGAMON

International Journal of Heat and Mass Transfer 43 (2000) 3105–3118

International Journal of HEAT and MASS TRANSFER

www.elsevier.com/locate/ijhmt

Convective trees of fluid channels for volumetric cooling

Adrian Bejan*, Marcelo R. Errera

Department of Mechanical Engineering and Materials Science, Duke University, Box 90300, Durham, NC 27708-0300, USA

Received 1 March 1999; received in revised form 25 October 1999

Abstract

This paper describes the geometric optimization of the internal structure of a volume that generates heat at every point and is cooled by a single stream. According to the constructal method, the optimization of the cooling design is organized in a sequence of steps that begins with the smallest volume element and continues with larger assemblies (constructs) of previously optimized building blocks. Optimized at each level of assembly are the external shape of the construct and the relative thickness of each duct for fluid flow. It is shown that in the end the fluid channels form a tree network that cools every point of the given volume. Length scales smaller than the thickness of the elemental volume are reached by conduction through the solid heat-generating material. Two fluid channel geometries are optimized: parallel-plate channels and round tubes.

1. The problem of volumetric cooling by convection

Constructal tree networks are flow paths deduced from one principle: the minimization of the global resistance to flow between a single point (source, or sink) and a finite-size volume, subject to global and local constraints [1]. Resistance minimization is performed consistently at every volume scale, and is subjected to the constraints of fixed total volume, fixed-volume fraction allocated to channels (tree links), and local temperatures that must not exceed the hot-spot limit. The medium is heterogeneous: the resistance to flow through the channels is considerably smaller than the resistance to flow through the material that fills the spaces between channels. Access between the single point and every point of the finite-size volume is made eventually through the diffusive-type flow that bathes the interstitial spaces.

The constructal optimization of volume-to-point access was first proposed in the context of pure heat conduction [1], where the channels are inserts of high thermal conductivity in a background medium (the interstitial material), which has lower thermal conductivity. The volume generates heat at every point, and is cooled from a single point (the sink). The method was since extended to fluid flow [2], by recognizing the heterogeneity associated with low-resistance flow through tubes embedded through a diffusive material with higher resistance (e.g., Darcy flow). Additional demonstrations and extensions of the method are reviewed in [3].

The method has its origin in the cooling of electronics, even though it has diverse applications that go beyond heat transfer, e.g., physiology, river morphology, and electrical engineering. Its development was stimulated by the trend toward minituarization of electronics cooling [4–7]. An essential contribution of recent advances in electronics cooling was to show that the global thermal resistance of a heat-generating volume can be optimized *geometrically*. The heat-flow path can be arranged optimally in space: this is a uni-

* Corresponding author. Tel.: +1-919-660-5310; fax: +1-919-660-8963.

E-mail address: abejan@duke.edu (A. Bejan).

0017-9310/00/$ - see front matter
PII: S0017-9310(99)00353-1

Nomenclature

A	area, m^2
c_P	specific heat at constant pressure, J/kg K
C	constant, Eq. (28)
D	thickness of fluid channel, m
H	volume height, m
k_0	solid thermal conductivity, W/m K
L	volume length, m
$\dot{m}'$	mass flow rate per unit length, kg/s m
$\dot{m}''$	mass flow rate per unit area, kg/s m^2
M	dimensionless mass flow rate, Eq. (4)
$\hat{M}$	dimensionless mass flow rate, Eq. (40)
n	number of constituents
Nu	Nusselt number
P_H	high pressure, Pa
P_L	low pressure, Pa
q'''	volumetric heat generation rate, W/m^3
t_1	thickness, m
T	temperature, K
T_0	initial fluid temperature, K
T_w	wall temperature, K
V	volume, m^3
x	longitudinal coordinate, m

Greek symbols

ΔP	pressure drop, Pa
ν	kinematic viscosity, m^2/s
ϕ	volume fraction allocated to fluid channels

Superscripts

~	dimensionless notation, Eq. (3)
^	dimensionless notation, Eq. (39)
-	average, Eq. (29)

Subscripts

0	elemental volume
1	first construct
2	second construct
m	minimized once
mm	minimized twice
opt	optimum
out	outlet
peak	peak, hot spot

fying characteristic of some of the most fundamental contributions to the cooling of electronics [8–10].

In this paper, we consider a fundamentally new application of the constructal method: the cooling of a solid heat-generating volume when the channels (the tree links) are ducts with fluid flow, not high-conductivity solid inserts. The optimization will balance the conduction through the solid interstices with the convection along the ducts. Out of this balance, the internal architecture of the volume with tree channels for volumetric cooling will result. The present problem may be viewed as a superposition of the pure heat conduction [1] and pure fluid flow [2] problems proposed earlier.

The fundamental problem proposed in this paper can be stated with reference to Fig. 1. The two-dimensional space HL generates heat volumetrically at the rate q''' (W/m^3), which is uniform. The temperature in this space cannot exceed a prescribed level, T_{peak}. The coolant is a stream of single-phase fluid $\dot{m}'$ (kg/s m) and initial temperature T_0. The objective is to cool every point of the volume, to maximize the overall thermal conductance $q'''HL/(T_{peak} - T_0)$, and to accomplish this task with minimal pumping power. This new problem and its geometric solution have fundamental implications not only in heat transfer (e.g., electric windings, electronic packages) but also in biology and the thermodynamics of nonequilibrium systems [3]. Additional applications are discussed in Section 8.

To see the direction of the geometric approach used in this paper, imagine the "ultimate" design in which the $\dot{m}'$ stream is distributed uniformly over H, and flows in the L direction while bathing every point of the HL space. This arrangement requires the use of two headers (thick black lines in Fig. 1), one upstream, to spread the $\dot{m}'$ stream, and the other downstream, to reconstitute the $\dot{m}'$ stream. It also requires a sufficiently refined porous structure (e.g., set of small parallel channels) through which the stream sweeps the entire HL space, from left to right. Such a flow sweeps the hot spots of the heat generating material (T_{peak}) to the right extremity of the HL space. When the porous structure is sufficiently fine, the peak temperature of the material is approximately the same as the peak bulk temperature of the permeating fluid. The latter occurs in the exit plane, such that the first law for the HL control volume can be written as

$$\dot{m}' c_P (T_{peak} - T_0) = q''' HL \tag{1}$$

This form is correct if the coolant exhibits ideal gas behavior with nearly constant c_P, or incompressible fluid behavior with moderate pressure changes. Eq. (1) shows that the overall conductance $q'''HL/(T_{peak} - T_0)$ is synonymous to the capacity flow rate $\dot{m}' c_P$. In an electronic package (HL), the largest amount of circuitry installed (q''') and the highest permissible tem-

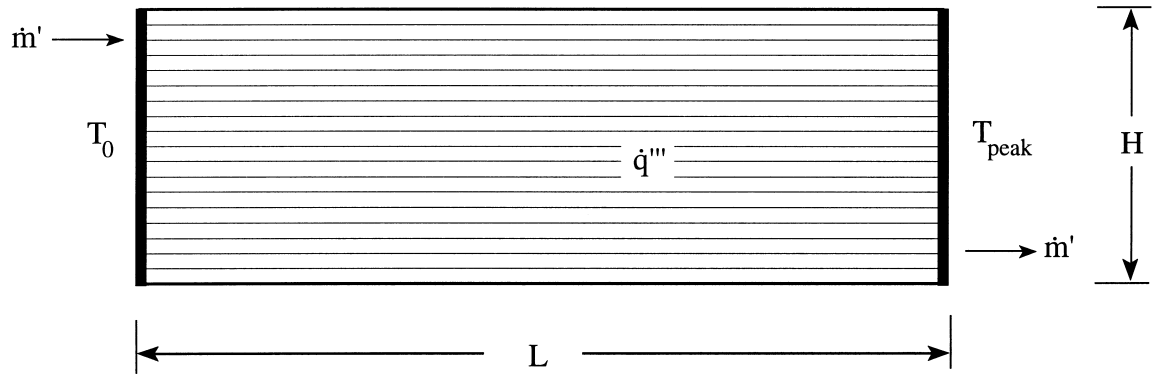

Fig. 1. Space with uniform volumetric heat generation and unidirectional permeating flow.

perature are dictated by materials, manufacturing and electrical engineering considerations. Once fixed, the overall thermal conductance fixes the coolant flow rate, or the distributed bathing flow rate $\dot{m}'' = \dot{m}'/H$.

In summary, the ultimate design described by Eq. (1) is a constant-$\dot{m}''$ design that would require a fine structure and, necessarily, a high pressure drop. In the following analysis, we investigate the possibilities of meeting the objectives of Eq. (1) by using flow paths with smaller pressure drops, and with hot spots that are distributed more uniformly over the volume. We base this search on the recently demonstrated constructal method [1–3], which showed that paths with lower overall resistance are achieved when their geometry (layout) is optimized, and when their internal complexity is increased. Such paths form tree networks.

2. The elemental volume

Regardless of which fluid-flow network is chosen, the first leg of the path followed by the flow of heat will always be one of conduction (thermal diffusion) through the solid heat generating material. An elemental volume scale exists where the heat conducted out of the material is swept away by the first stream of coolant. This smallest scale is called *elemental volume*, and is represented by the rectangle H_0L_0 shown in Fig. 2. Only one fluid channel (D_0) penetrates this volume. The smallness of the elemental size (the area $A_0 = H_0L_0$) is fixed by manufacturing considerations: smaller H_0L_0 sizes lead to better designs. The external shape (H_0/L_0) and the internal opening (D_0/H_0) are the two degrees of freedom of the elemental geometry.

All the heat generated inside the elemental volume ($q'''H_0L_0$) is convected away by the elemental stream that flows through the D_0 channel. The flow rate of this stream is $\dot{m}_0' = \dot{m}''H_0$, where $\dot{m}''$ is a constant. In Fig. 2, the rectangular boundary $H_0 \times L_0$ is assumed to be adiabatic with the exception of the coldest spot (T_0) that occurs in the immediate vicinity of the inlet to the D_0 channel. The hot spots (T_{peak}) occur in the two corners that are situated farthest from the inlet.

An analytical expression for the peak excess temperature ($T_{\text{peak}} - T_0$) can be developed when k_0 is small, and the aspect ratio H_0/L_0 is sufficiently smaller than 1 such that the conduction through the heat-generating material (k_0) is oriented perpendicular to the fluid channel. If we also assume that $D_0 \ll H_0$, the temperature drop between the hot-spot corner (T_{peak}) and the wall spot near the channel outlet in Fig. 2 is $T_{\text{peak}} - T_{\text{w}} = q'''H_0^2/(8k_0)$, in accordance with the steady-conduction analysis reported in [1]. The increase experienced by the bulk temperature of the stream from inlet to outlet is $T_{\text{out}} - T_0 = q'''H_0L_0/(\dot{m}_0'c_{\text{P}})$. There is also a temperature difference between the bulk temperature T_{out} and the duct wall temperature (T_{w}) in the plane of the outlet: temperature differences of this kind are neglected in this study based on the assumption that the flow is fully developed and the channel spacing is sufficiently small. The necessary validity condition is discussed in the last paragraph of this section.

In conclusion, the peak excess temperature is given by a two-term expression ($T_{\text{peak}} - T_0 = (T_{\text{peak}} - T_{\text{w}}) + (T_{\text{w}} - T_0)$) that can be nondimensionalized in the form of the overall resistance of the elemental volume,

$$\Delta\tilde{T}_0 = \frac{\tilde{H}_0}{8\tilde{L}_0} + \frac{1}{M\tilde{H}_0} \tag{2}$$

where

$$\left(\tilde{H}_0, \tilde{L}_0\right) = \frac{(H_0, L_0)}{A_0^{1/2}} \quad \Delta\tilde{T}_0 = \frac{T_{\text{peak}} - T_0}{q'''A_0/k_0} \tag{3}$$

$$M = \dot{m}''c_{\text{P}}A_0^{1/2}/k_0, \text{ constant} \tag{4}$$

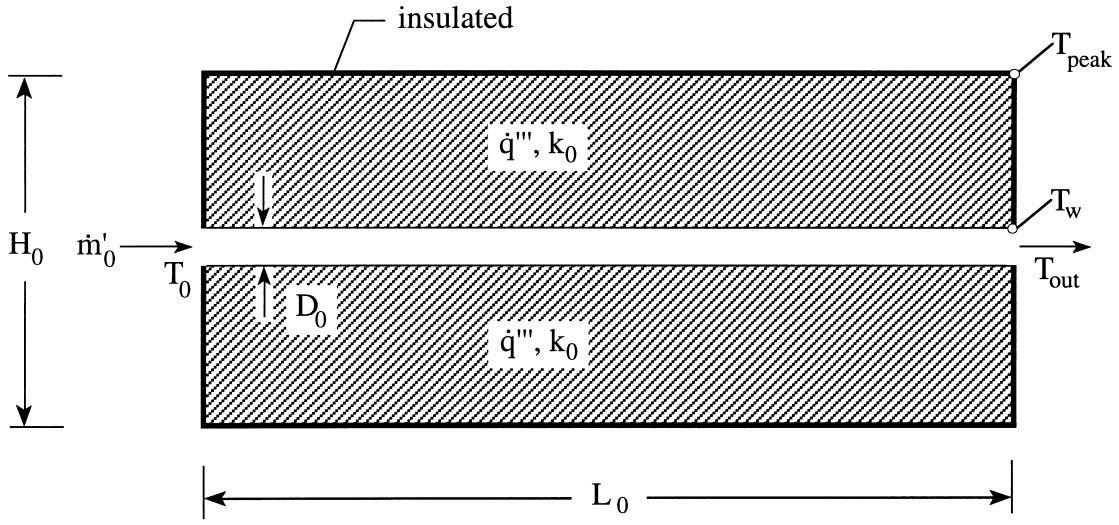

Fig. 2. Elemental volume with heat generation, conduction, and single-stream cooling.

In this notation, the size constraint $H_0L_0 = A_0$ becomes $\tilde{H}_0\tilde{L}_0 = 1$. The right-hand side of Eq. (2) is equal to $(\tilde{H}_0^2/8) + 1/(M\tilde{H}_0)$, and shows that the overall resistance $\Delta\tilde{T}_0$ can be minimized with respect to the external shape parameter $\tilde{H}_0$. The results are

$$\tilde{H}_{0,\,\mathrm{opt}} = \left(\frac{4}{M}\right)^{1/3} \quad \tilde{L}_{0,\,\mathrm{opt}} = \left(\frac{M}{4}\right)^{1/3} \tag{5}$$

$$\left(\frac{H_0}{L_0}\right)_{\mathrm{opt}} = \left(\frac{4}{M}\right)^{2/3} \quad \Delta\tilde{T}_{0,\,\mathrm{min}} = \frac{3}{2^{5/3}M^{2/3}} \tag{6}$$

The optimal external shape $(H_0/L_0)_{\mathrm{opt}}$, which is independent of the channel size D_0, is worth noting. The elemental volume is more elongated when the flow parameter M is large, i.e., when $\dot{m}''$ and A_0 are large and k_0 is small. The starting assumption that $H_0/L_0 < 1$ means that the above solution is valid when $M > 4$. The assumption that $T_w - T_{out}$ is negligible (relative to $T_{peak} - T_w$) means that $D_0/H_0 \ll Nuk/k_0$, where k is the thermal conductivity of the fluid and Nu is a dimensionless constant of order 1 (the Nusselt number for fully developed laminar flow in a parallel-plate channel). This last inequality comes from writing $T_w - T_{out} \ll T_{peak} - T_w$ and the definitions $Nu = 2D_0h/k$, $h = q''/(T_w - T_{out})$ and $q'' = q'''H_0/2$.

3. The first construct

The original space HL of Fig. 1 can be filled with the necessary number (HL/A_0) of elemental volumes of the type that was optimized in the preceding section. The remaining question is how to connect these building blocks so that each is bathed by a portion of the original stream $\dot{m}'$. The challenge is to connect the elements in a way that minimizes the overall pressure drop experienced by the $\dot{m}'$ stream.

The first step in this direction is shown in Fig. 3. We take a number (n_1) of elemental volumes and stack them into a *first construct* of dimensions $H_1 = L_{0,\,\mathrm{opt}}$ and $L_1 = n_1H_{0,\,\mathrm{opt}}$. The elements are fed with cold fluid from a channel of length $L_1 - H_0/2$ and thickness $D_1/2$. A similar channel collects the elemental streams and reconstitutes the total stream of the first construct, $\dot{m}_1' = n_1\dot{m}_0'$.

The total pressure difference between inlet and outlet of the first construct is

$$\Delta P_1 = \Delta P_0 + \Delta P_{D_1/2} \tag{7}$$

If the flow through each elemental channel is in the Hagen–Poiseuille regime, the pressure drop across one elemental volume is $\Delta P_0 = 12\nu L_{0,\,\mathrm{opt}}\dot{m}_0'/D_0^3$. The second term in Eq. (7) refers to the pressure drop along one of the $D_1/2$-wide channels. For reasons that will be made clear in the next section, the outer side of each $D_1/2$ channel is modeled as a zero-shear surface. The flow through the $D_1/2$ channel is also in the Poiseuille regime. When n_1 is sufficiently large, the flow rate varies linearly along the channel, from the total value $\dot{m}_1'$ at one end, to zero at the opposite end. Under these circumstances, it can be shown that the pressure drop integrated along the $D_1/2$ channel is equal to $12\nu L_1\dot{m}_1'/D_1^3$. The total pressure drop formula (7) can be rewritten as a dimensionless overall flow resistance

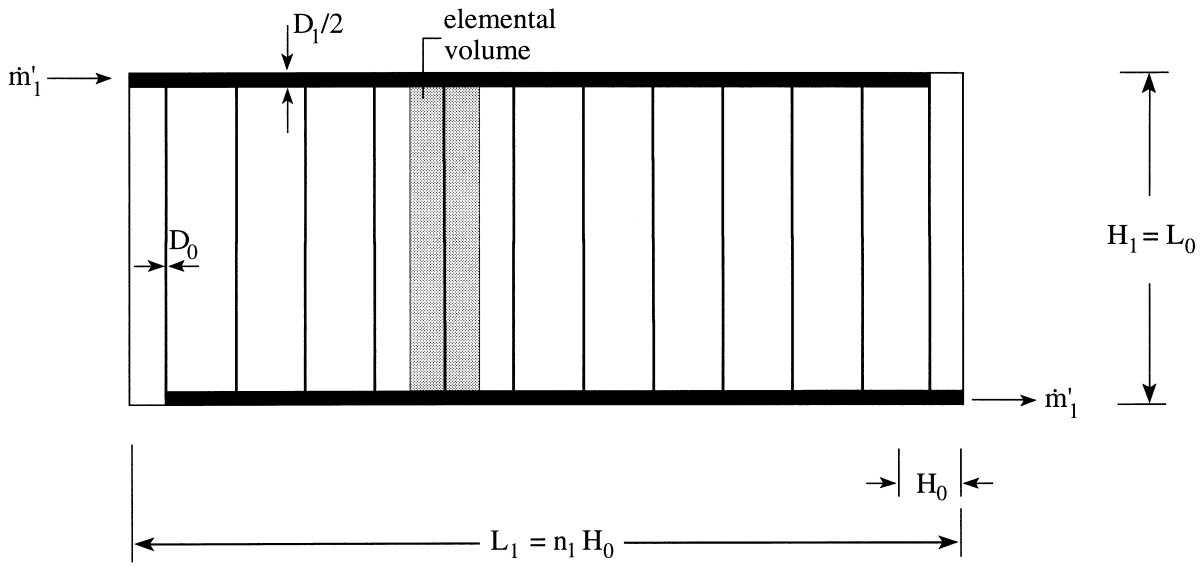

Fig. 3. First construct containing n_1 elemental volumes.

$$\Delta\tilde{P}_1 = \frac{\Delta P_1 A_0}{12\nu\dot{m}_1'} = \frac{\tilde{L}_{0,\,\mathrm{opt}}}{n_1\tilde{D}_0^3} + \frac{n_1\tilde{H}_{0,\,\mathrm{opt}}}{\tilde{D}_1^3} \tag{8}$$

Consider now the effect of the number of constituents (n_1) on the overall resistance of the first construct. Both ΔP_1 and $\dot{m}_1'$ increase as n_1 increases. The interesting effect is that there is an optimal n_1 — an optimal size — for minimal resistance at the first construct level,

$$n_{1,\,\mathrm{opt}} = \left(\frac{L_0}{H_0}\right)_{\mathrm{opt}}^{1/2}\left(\frac{D_1}{D_0}\right)^{3/2} \tag{9}$$

$$\Delta\tilde{P}_{1,\,\mathrm{min}} = 2\left(\frac{A_0}{D_1 D_0}\right)^{3/2} \tag{10}$$

In this first optimization step, resistance minimization is achieved through optimal growth, i.e., through the aggregation of an optimal number of elements. The expression for $\Delta\tilde{P}_{1,\,\mathrm{min}}$ can be minimized further by increasing D_1 and D_0. These changes are not without limits, because the space occupied by fluid channels is taken away from space that could have been occupied by heat generating material. We account for this limitation through a total fluid volume constraint,

$$A_{1,\,\mathrm{fluid}} = n_1 D_0 L_{0,\,\mathrm{opt}} + 2\frac{D_1}{2}L_1 \tag{11}$$

where $A_{1,\,\mathrm{fluid}}$ is a specified (small) fraction of the total volume of the first construct, $\phi_1 = A_{1,\,\mathrm{fluid}}/(H_1 L_1)$. The fluid-volume constraint (11) becomes

$$\phi_1 = \frac{D_0}{H_{0,\,\mathrm{opt}}} + \frac{D_1}{L_{0,\,\mathrm{opt}}},\ \text{constant} \tag{12}$$

The minimization of the $\Delta\tilde{P}_{1,\,\mathrm{min}}$ expression (10) with respect to either D_1 or D_0, and subject to the constraint (12), yields

$$D_{0,\,\mathrm{opt}} = \frac{\phi_1}{2}H_{0,\,\mathrm{opt}} \quad D_{1,\,\mathrm{opt}} = \frac{\phi_1}{2}L_{0,\,\mathrm{opt}} \tag{13}$$

$$\left(\frac{D_1}{D_0}\right)_{\mathrm{opt}} = \left(\frac{M}{4}\right)^{2/3} \quad \left(\frac{H_1}{L_1}\right)_{\mathrm{opt}} = \left(\frac{M}{4}\right)^{-2/3}$$
$$\Delta\tilde{P}_{1,\,\mathrm{mm}} = \frac{16}{\phi_1^3} \tag{14}$$

The subscript 'mm' indicates that the overall resistance $\Delta\tilde{P}_{1,\,\mathrm{mm}}$ has been minimized twice. Combining $(D_1/D_0)_{\mathrm{opt}}$ with Eqs. (9) and (6), we find the optimal number of constituents in the first construct,

$$n_{1,\,\mathrm{opt}} = \left(\frac{M}{4}\right)^{4/3} \tag{15}$$

Since the analysis is valid for $M \gg 4$ (Section 2), we conclude that $n_{1,\,\mathrm{opt}} \gg 1$, and in this way, we validate the assumption on which Fig. 3 was based.

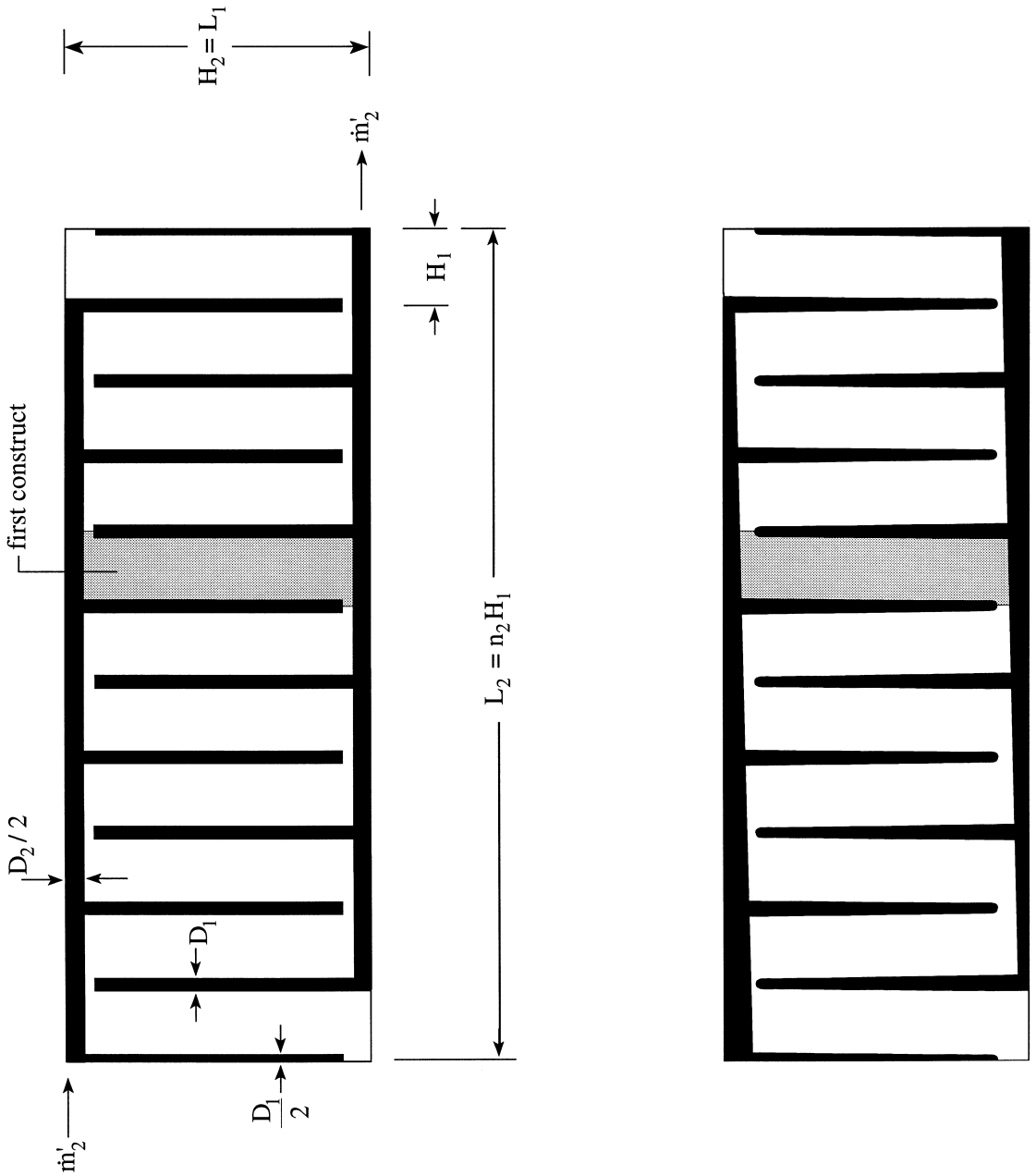

Fig. 4. Second construct containing n_2 first constructs: uniform-thickness channels (top), and tapered channels (bottom).

4. The second construct

Even larger portions of the original volume of Fig. 1 can be filled by connecting together a number (n_2) of first constructs optimized in the preceding section. The resulting geometry is the *second construct* shown in Fig. 4, where $H_2L_2 = n_2H_1L_1$, $H_2 = L_1$ and $L_2 = n_2H_1$. Note the alternating pattern in which we added first constructs to Fig. 4: this time, we "flipped" the design of Fig. 3 so that in the second construct two $D_1/2$-wide channels come together to form a single D_1-wide channel. The midplane of each D_1 channel is the outer (zero-shear) surface modeled in the preceding section.

The total flow rate of the second construct is equal to the sum of the flow rates handled by the first constructs, $\dot{m}_2' = n_2\dot{m}_1'$. The $\dot{m}_2'$ stream is first distributed and, later, collected by channels of length L_2 and width $D_2/2$. The outer planes of the two $D_2/2$ channels are modeled as zero-shear surfaces. The total pressure drop experienced by the $\dot{m}_2'$ stream is

$$\Delta P_2 = \Delta P_{1,\,\mathrm{mm}} + \Delta P_{D_2/2} \tag{16}$$

where $\Delta P_{1,\,\mathrm{mm}}$ can be derived from Eq. (14). The second term on the right-hand side of Eq. (16) can be derived by making the same assumptions as for $\Delta P_{D_1/2}$ in the preceding section, and the result is $12\nu L_2\dot{m}_2'/D_2^3$. The nondimensional resistance that follows from Eq. (16) is

$$\Delta\tilde{P}_2 = \frac{\Delta P_2 A_0}{12\nu\dot{m}_2'} = \frac{16}{n_2\phi_1^3} + \frac{n_2H_1A_0}{D_2^3} \tag{17}$$

The minimization of $\Delta\tilde{P}_2$ with respect to n_2 yields

$$n_{2,\,\mathrm{opt}} = \left(\frac{16D_2^3}{\phi_1^3A_0H_1}\right)^{1/2} \tag{18}$$

$$\Delta\tilde{P}_{2,\,\mathrm{min}} = \frac{8(M/4)^{1/6}}{\tilde{D}_2^{3/2}\phi_1^{3/2}} \tag{19}$$

where $\tilde{D}_2 = D_2/A_0^{1/2}$. The second minimization of the overall flow resistance is conducted subject to the total fluid space constraint

$$A_{2,\,\mathrm{fluid}} = n_2A_{1,\,\mathrm{fluid}} + 2\frac{D_2}{2}L_2 \tag{20}$$

Let ϕ_2 be the specified fluid-volume fraction in the second construct, $\phi_2 = A_{2,\,\mathrm{fluid}}/(H_2L_2)$. The nondimensional version of Eq. (20) is then

$$\phi_2 = \phi_1 + \frac{4}{M}\tilde{D}_2,\ \text{constant} \tag{21}$$

The minimization of $\Delta\tilde{P}_{2,\,\mathrm{min}}$ with respect to $\tilde{D}_2$ and ϕ_1, and subject to the constraint (21), yields

$$\phi_{1,\,\mathrm{opt}} = \frac{\phi_2}{2} \quad \tilde{D}_{2,\,\mathrm{opt}} = \frac{M}{8}\phi_2 \tag{22}$$

$$\Delta\tilde{P}_{2,\,\mathrm{mm}} = \frac{512}{2^{1/3}M^{4/3}\phi_2^3} \tag{23}$$

In view of Eq. (18) and the double optimization performed in the preceding section, the optimized second construct is also characterized by

$$n_{2,\,\mathrm{opt}} = 4\left(\frac{M}{4}\right)^{4/3} = 4n_1 \tag{24}$$

$$\left(\frac{H_2}{L_2}\right)_{\mathrm{opt}} = \frac{1}{2}\left(\frac{D_1}{D_2}\right)_{\mathrm{opt}} = \frac{1}{4}\left(\frac{4}{M}\right)^{2/3} = \frac{1}{4}\left(\frac{H_1}{L_1}\right)_{\mathrm{opt}} \tag{25}$$

5. Optimally tapered flow channels

In the analyses presented in Sections 3 and 4, we assumed that the central channel of each new construct has a uniform thickness, D_1 and, respectively, D_2. We made this choice for the sake of simplicity, in order to highlight each step of assembly (growth, aggregation), which is followed by geometric optimization. The constant-thickness assumption is not compatible with the requirement that the collecting channel must receive a uniform flow rate per unit channel length. To see why, recall that in the first construct of Fig. 3, the flow rate must be the same through each D_0 channel, and, consequently, the flow rate through each $D_1/2$ channel must vary linearly along L_1, from $\dot{m}_1'$ to zero,

$$\dot{m}_{1,\,x}' = \dot{m}_1'\left(1 - \frac{x}{L_1}\right) \tag{26}$$

This expression refers to the top $D_1/2$ channel of Fig. 3, where $x = 0$ marks the entrance. The local pressure gradient along this channel is

$$-\frac{\mathrm{d}P_{\mathrm{H}}}{\mathrm{d}x} = 24\nu\frac{\dot{m}_{1,\,x}'}{D_1^3} \tag{27}$$

The distribution of high pressure $P_{\mathrm{H}}(x)$ depends on the function $D_1(x)$, which must be determined. If D_1 is a constant, then $P_{\mathrm{H}}(x)$ has a parabolic shape. If D_1 is tapered as $(1 - x/L_1)^{1/3}$, then $P_{\mathrm{H}}(x)$ varies linearly as shown with solid lines in Fig. 5.

Relations similar to Eqs. (26) and (27) hold for the distribution of low pressure, $P_{\mathrm{L}}(x)$, along the receiving $D_1/2$ channel. The pressure difference that drives the flow through each elemental (D_0) channel is $P_{\mathrm{H}}(x) -$

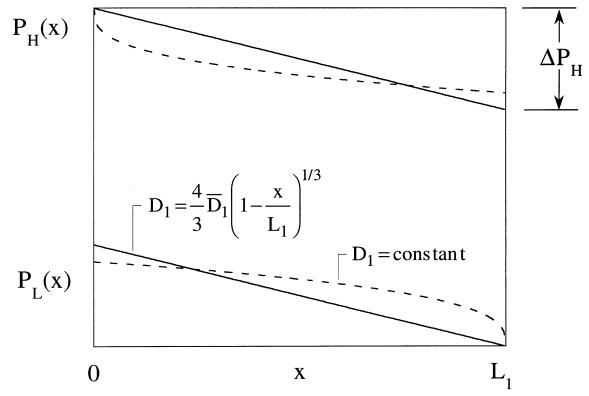

Fig. 5. The pressure distribution along the $D_1/2$-thick channels of the first construct.

$P_L(x)$. The elemental flow rate is independent of x only when $P_H(x) - P_L(x)$ is a constant, i.e., when $P_H(x)$ and $P_L(x)$ vary linearly. In conclusion, the ratio $\dot{m}_{1,x}/D_1^3$ must be a constant in Eq. (27) and, in view of Eq. (26),

$$D_1(x) = C\left(1 - \frac{x}{L_1}\right)^{1/3} \tag{28}$$

The constant C accounts for the volume of the D_1 channel, or for the result of averaging $D_1(x)$ from $x = 0$ to L_1,

$$\bar{D}_1 = \frac{1}{L_1}\int_0^{L_1} D_1(x)\,\mathrm{d}x = \frac{3}{4}C \tag{29}$$

The pressure drop along the channel length L_1, which results from Eq. (27), is

$$\frac{\Delta P_H}{L_1} = \frac{81}{8}\nu\frac{\dot{m}_1'}{\bar{D}_1^3} \tag{30}$$

The optimal power-law tapering of the channel, Eq. (28), applies to every subsequent-level channel that must receive uniform flow rate per unit length. The lower part of Fig. 4 shows the tapered versions of $D_1(x)$ and $D_2(x)$, which can be compared directly with the uniform-D_1 and -D_2 drawing shown in the upper part of the figure. The optimal dimensions and aspect ratios of the constructs with tapered collecting channels agree closely with the results presented in Sections 3 and 4. The analysis can be repeated by starting with the line above Eq. (8), in which the pressure drop along the $D_1/2$ channel of the first construct ($12\nu L_1\dot{m}'/D_1^3$, or Eq. (27)) is now replaced by $2(3/2)^4\nu\dot{m}_1'/\bar{D}_1^3$, cf. Eq. (30). In other words, the place of D_1 is taken by $\bar{D}_1$, and the factor 12 is replaced by $2(3/2)^4$. The main features of the optimized first construct are now described by

$$\left(\frac{\bar{D}_1}{D_0}\right)_{\text{opt}} = \left(\frac{M}{4}\right)^{2/3}$$
$$\left(\frac{H_1}{L_1}\right)_{\text{opt}} = 2^{1/2}\left(\frac{3}{4}\right)^{3/2}\left(\frac{4}{M}\right)^{2/3} \tag{31}$$

$$n_{1,\text{opt}} = 2^{-1/2}\left(\frac{4}{3}\right)^{3/2}\left(\frac{M}{4}\right)^{4/3}$$
$$\Delta\tilde{P}_{1,\text{mm}} = 2^{1/2}\left(\frac{3}{4}\right)^{3/2}\frac{16}{\phi_1^3} \tag{32}$$

These results can be compared with Eqs. (14) and (15) to see the close agreement, i.e., that the uniform-D_1 analysis is an approximate (and more direct) method of determining the optimized geometry.

The optimization of the second construct (Section 4) can be repeated by starting with the line above Eq. (17), in which $12\nu L_2\dot{m}_2'/D_2^3$ is replaced by $(81/8)\nu L_2\dot{m}_2'/\bar{D}_2^3$. Eqs. (23)–(25) are replaced by

$$\left(\frac{\bar{D}_2}{\bar{D}_1}\right)_{\text{opt}} = \frac{2^{7/2}}{3^{3/2}}\left(\frac{M}{4}\right)^{2/3}$$
$$\left(\frac{H_2}{L_2}\right)_{\text{opt}} = \frac{3^{3/2}}{2^{9/2}}\left(\frac{4}{M}\right)^{2/3} \tag{33}$$

$$n_{2,\text{opt}} = \frac{2^7}{3^3}\left(\frac{M}{4}\right)^{4/3} \qquad \Delta\tilde{P}_{2,\text{mm}} = \frac{3^3}{2^5}\frac{512}{2^{1/3}M^{4/3}\phi_2^3} \tag{34}$$

Combining the revised analyses of the first and second constructs, we find that

$$n_{2,\text{opt}} = \frac{2^{5/2}}{3^{3/2}}4n_{1,\text{opt}} \quad \text{and}$$
$$\left(\frac{H_2}{L_2}\right)_{\text{opt}} = \left(\frac{2}{3}\right)^{3/2}\left(\frac{\bar{D}_1}{\bar{D}_2}\right)_{\text{opt}} = \frac{1}{4}\left(\frac{H_1}{L_1}\right)_{\text{opt}} \tag{35}$$

which agree within 20% with the uniform-(D_1, D_2) results of Eqs. (24) and (25).

Fig. 6 shows, in color, the layout of the first, second and third constructs. Blue indicates colder channels that bring in the coolant and distribute it through the given volume. Red indicates the warmed up fluid that is collected and led out of the volume. The elemental channels change color in the middle, from blue to red, to suggest that at the elemental level each stream warms up while absorbing the generated heat that diffuses through the solid, which is shown in yellow. As the constructs compound themselves, the cooled volume acquires a structure similar to that of a vascu-

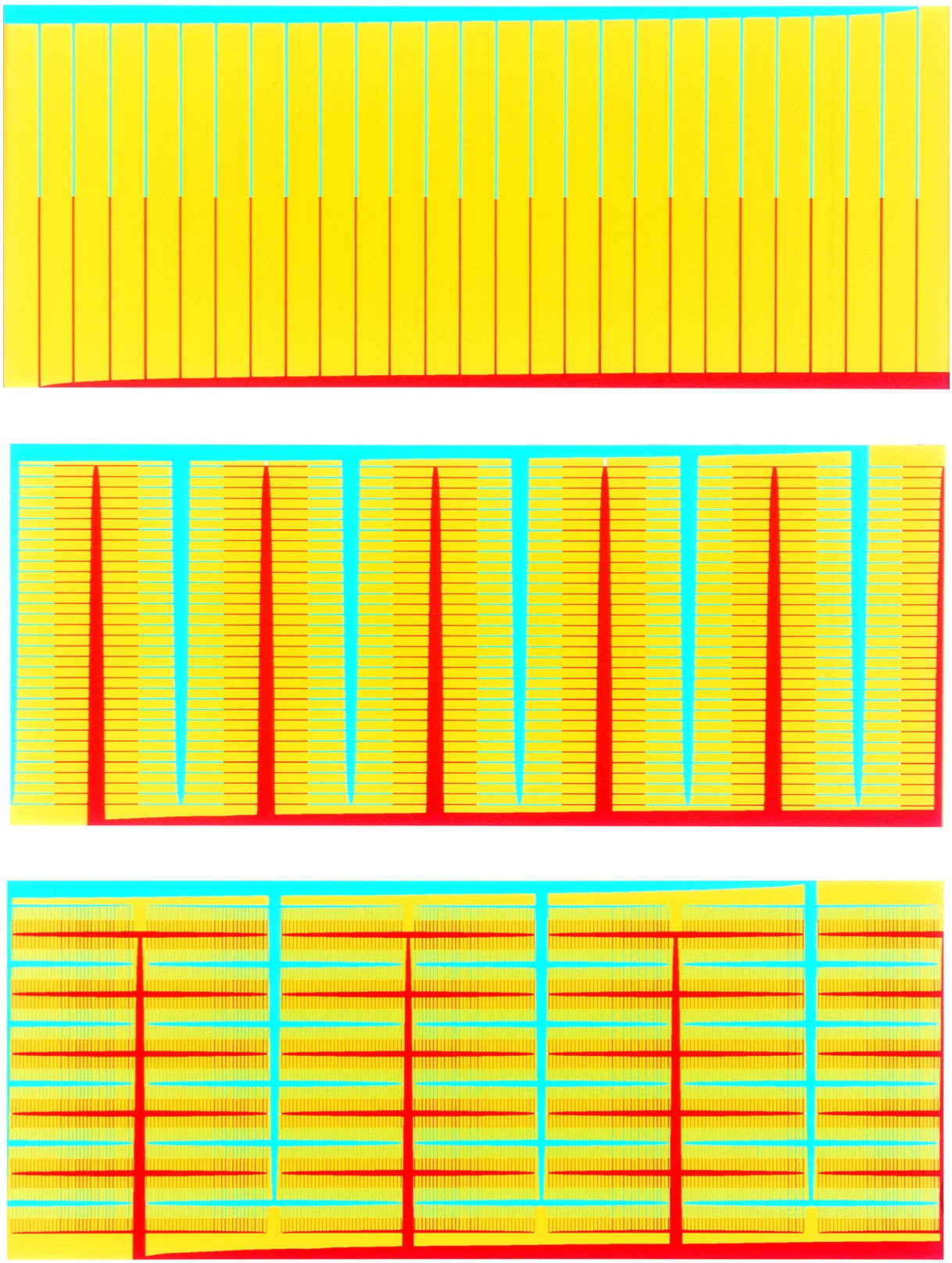

Fig. 6. Color displays of inflowing (blue) and outflowing (red) streams in the first construct (top), second construct (middle), and third construct (bottom).

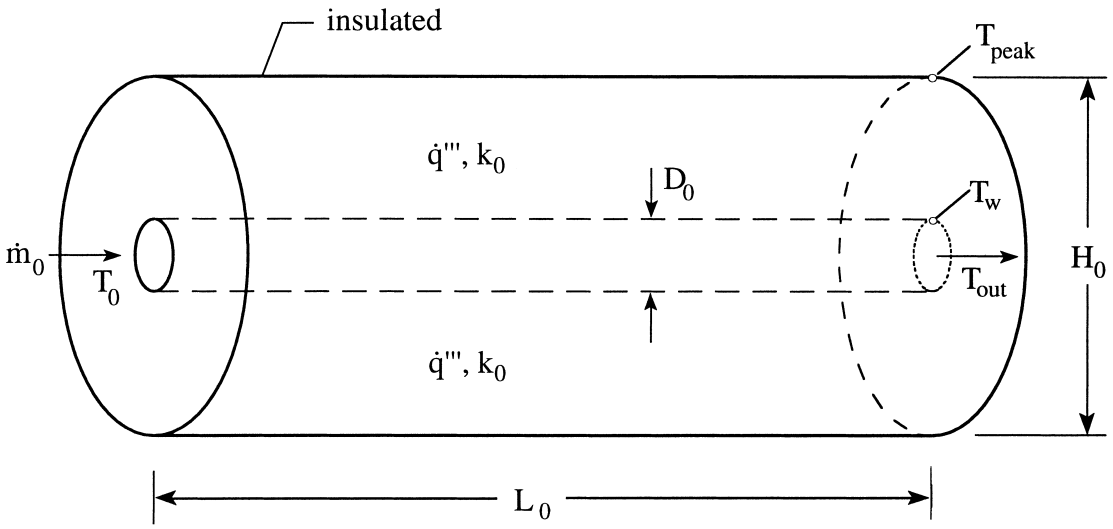

Fig. 7. Elemental volume with radial symmetry and round channel.

larized tissue, where one tree network (arteries) meets another (veins) in every volume element of the tissue.

6. Higher order constructs

The optimization sequence illustrated at three levels of increasing complexity in the preceding sections (elemental volume, first construct, second construct) can be continued toward constructs of higher order, which will cover increasingly larger volumes. The analytical method would be the same as in Sections 3 and 4. The geometric results too would continue the trends that became visible as early as the second construct. Specifically, since this analytical course is valid when $M/4 > 1$, each new channel will be larger than the largest preceding channel size, with a width magnification factor of order $\bar{D}_{i+1}/\bar{D}_i \sim (M/4)^{2/3}$ for $i \geq 2$. The stepwise increase in channel width agrees qualitatively with the behavior of the corresponding solution for tree networks in pure heat conduction [1].

A trend that goes against the trees of heat conduction is the stepwise increase in the external slenderness ratio. In heat conduction, the higher order constructs were square or close to square. In the present problem, if we look at Eqs. (6), (31) and (35), we anticipate that the ratios H_{i+1}/L_{i+1} will continue to be of order $(4/M)^{2/3} < 1$, and that they will decrease in small steps as the constructs become larger. The point–volume–point flow schemes will have to fit in more and more slender spaces, and this will interfere eventually with the outer constraints (boundary, shape) of the total volume that must be cooled. The only course of action left is to optimize the geometry of the shape-constrained system numerically, as shown for pure conduction in [1]. This is why, in this paper, we have not continued the analytical sequence beyond the second construct.

Another trend that is unlikely in pure heat conduction is shown by the first of Eq. (35): the number of constituents increases as the order of the construct increases. In the heat conduction tree, the number of constituents decreased until it reached 2 (dichotomy).

7. Round tubes

We illustrated the geometric optimization of the point–volume–point flow path in two dimensions, by assuming that each channel is a fissure with parallel walls. The same method can be used to optimize designs with channels of round cross-section. The start of this optimization sequence is based on Fig. 7. The elemental level is defined by the smallest channel, which has the diameter D_0 and length L_0. As elemental volume we consider the cylinder of diameter H_0. Heat is generated in the solid annulus of thermal conductivity k_0.

To construct the analytical expression for the thermal resistance of the elemental volume, we assume that $H_0 < L_0$, and note that $T_{peak} - T_0 = (T_{peak} - T_w) + (T_w - T_0)$. The temperature difference in the radial direction is derived from the solution to the problem of steady conduction in an annular space with uniform heat generation rate,

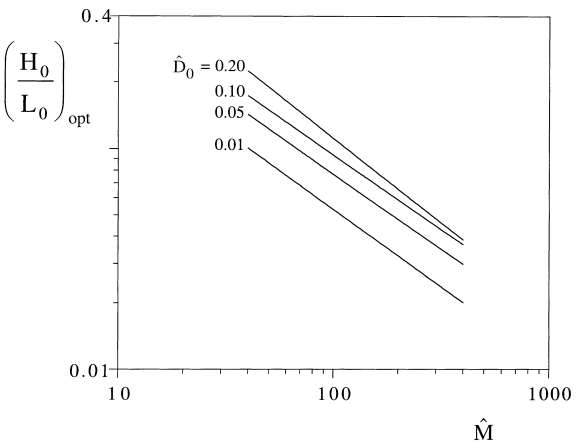

Fig. 8. The optimal shape of the elemental volume with round channel.

$$T_{\text{peak}} - T_{\text{w}} = \frac{q''' H_0}{16 k_0}\left[2\ln\frac{H_0}{D_0} + \left(\frac{D_0}{H_0}\right)^2 - 1\right] \tag{36}$$

The flow rate of the elemental stream is $\dot{m}_0 = \dot{m}''(\pi/4)H_0^2$. The longitudinal temperature increase experienced by the stream is

$$T_{\text{out}} - T_0 = \frac{\pi}{4}\left(H_0^2 - D_0^2\right)L_0 q'''/(\dot{m}_0 c_{\text{P}}) \tag{37}$$

Next, we assume that $T_{\text{out}} - T_0 \cong T_{\text{w}} - T_0$, and add Eqs. (36) and (37). The resulting expression

$$\Delta\hat{T}_0 = \frac{\hat{L}_0}{\hat{M}}\frac{H_0^2 - D_0^2}{H_0^2} + \frac{\hat{H}_0^2}{16}\left[2\ln\frac{\hat{H}_0}{\hat{D}_0} + \left(\frac{\hat{D}_0}{\hat{H}_0}\right)^2 - 1\right] \tag{38}$$

has been nondimensionalized by using $V_0^{1/3}$ as length scale, where V_0 is the constant volume of the elemental system, $V_0 = (\pi/4)H_0^2 L_0$:

$$\left(\hat{H}_0, \hat{L}_0, \hat{D}_0\right) = \frac{(H_0, L_0, D_0)}{V_0^{1/3}} \quad \Delta\hat{T}_0 = \frac{T_{\text{peak}} - T_0}{q''' V_0^{2/3}/k_0} \tag{39}$$

$$\hat{M} = \dot{m}'' c_{\text{P}} V_0^{1/3}/k_0, \text{ constant} \tag{40}$$

The volume constraint $(\pi/4)\hat{H}_0^2\hat{L}_0 = 1$ and the known size of the smallest tube ($\hat{D}_0$) leave only one degree of freedom in the minimization of $\Delta\hat{T}_0$. The free parameter is $\hat{L}_0$ or $\hat{H}_0$, or the slenderness ratio H_0/L_0. We minimized $\Delta\hat{T}_0$ numerically and obtained the results shown in Fig. 8. The ratio $(H_0/L_0)_{\text{opt}}$ varies almost as $\hat{M}^{-1/2}$, which agrees qualitatively with the result for two-dimensional channels, Eq. (6). The data of Fig. 8 and the corresponding minimum resistance are, respectively, correlated within 2 and 1% by the expressions

$$\left(\frac{H_0}{L_0}\right)_{\text{opt}} \cong 2.37\hat{M}^{-0.556}\hat{D}_0^{0.248} \tag{41}$$

$$\Delta\hat{T}_{0,\,\text{min}} = 0.575\hat{M}^{-0.536}\hat{D}_0^{-0.264} \tag{42}$$

The first construct that can be made with the optimized elements is shown in Fig. 9. The collected stream $\dot{m}_1$ flows through half of a channel of diameter D_1. The elements form a slab of length L_1, height H_1 (= L_0) and thickness $t_1 = H_0$. The latter is an approximation, because n_1 parallel cylinders do not fill a parallelepiped completely. A better estimate for the slab thickness t_1 is obtained from the volume conservation argument $L_1 H_1 t_1 = n_1(\pi/4)H_0^2 L_0$ and $L_1 = n_1 t_1$, which yields $t_1 = (\pi/4)^{1/2}H_0$.

The calculation of the pressure drop ΔP_1 across the first construct follows the steps outlined in Section 3. We assume that D_1 and D_2 are fixed during the first phase of the optimization procedure. The pressure drop between inlet and outlet of the first construct (Fig. 9) is $\Delta P_1 = \Delta P_0 + \Delta P_{D_1}/2$. The flow is assumed to be in the Hagen–Poiseuille regime, therefore, the overall flow resistance is

$$\Delta\hat{P}_1 = \frac{\Delta P_1 \pi V_0}{128\dot{m}_1\nu} = \frac{\hat{L}_{0,\,\text{opt}}}{n_1\hat{D}_0^4} + n_1\frac{\hat{t}_{1,\,\text{opt}}}{\hat{D}_1^4} \tag{43}$$

The resistance can be minimized by selecting the number of constituents,

$$n_{1,\,\text{opt}} = \left(\frac{\hat{D}_1}{\hat{D}_0}\right)^2\left(\frac{\hat{L}_{0,\,\text{opt}}}{\hat{t}_{1,\,\text{opt}}}\right)^{1/2} \tag{44}$$

$$\Delta\hat{P}_{1,\,\text{min}} = \frac{2}{\hat{t}_{1,\,\text{opt}}\hat{D}_0^2\hat{D}_1^2} \tag{45}$$

In Eq. (45), we may replace $\hat{t}_{1,\,\text{opt}}$ by $(\pi/4)^{1/2}\hat{H}_{0,\,\text{opt}}$ to express $\Delta\hat{P}_{1,\,\text{min}}$ as a function of the shape, since $\hat{H}_{0,\,\text{opt}} = [4/\pi(\hat{H}_0/\hat{L}_0)_{\text{opt}}]$: we find that $\Delta\hat{P}_{1,\,\text{min}}$ varies nearly as $\hat{M}^{1/5}$ for a given $\hat{D}_0$.

Eq. (45) also shows that we may reduce the resistance further by increasing $\hat{D}_0$ and $\hat{D}_1$. These diameters are related through the fluid volume constraint

$$\phi_1 = \frac{V_{1,\,\text{fluid}}}{V_1} = \frac{\pi}{4}\hat{D}_0^2\hat{L}_{0,\,\text{opt}} + \frac{\pi}{4}\hat{D}_1^2\hat{t}_{1,\,\text{opt}}, \text{ constant} \tag{46}$$

The results of minimizing Eq. (45) with respect to $\hat{D}_0$ and $\hat{D}_1$ subject to Eq. (46), are

$$\hat{D}_{0,\,\text{opt}} \cong 0.714\phi_1^{1/2}\hat{H}_{0,\,\text{opt}} \tag{47}$$

$$\hat{D}_{1,\,\text{opt}} \cong 0.7\left(\frac{4}{\pi}\right)^{3/4}\phi_1^{1/2}\hat{H}_{0,\,\text{opt}}^{-1/2} \tag{48}$$

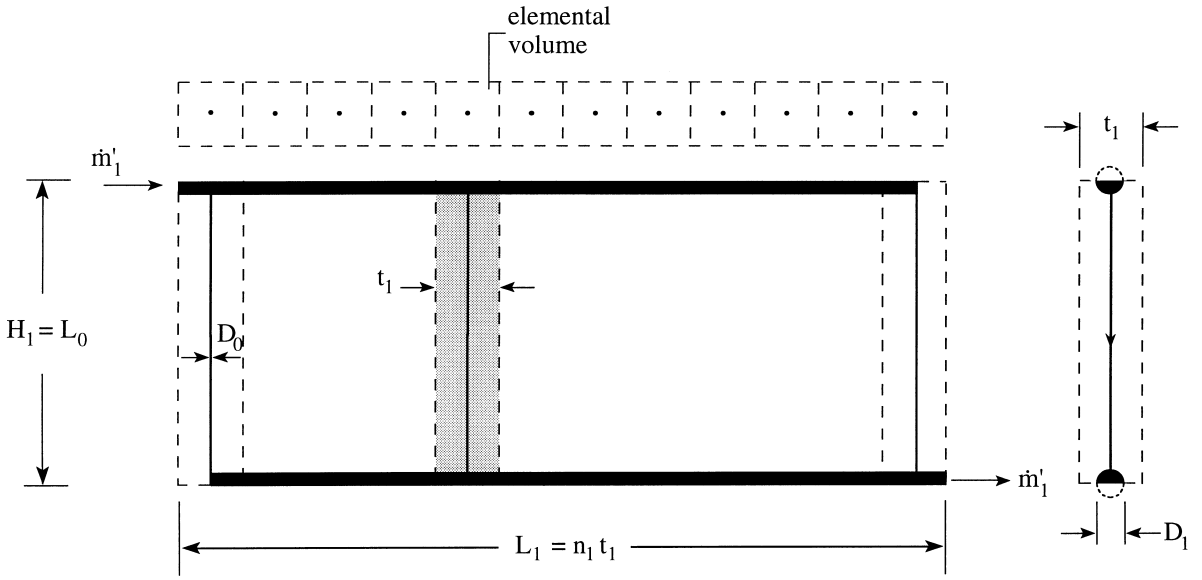

Fig. 9. First construct with channels with round cross-section.

These results can be combined with the $\hat{H}_{0,\,\mathrm{opt}}$ relation obtained at the elemental level (Eq. (41)),

$$\hat{D}_{0,\,\mathrm{opt}} \cong 1.04\hat{M}^{-0.202}\phi_1^{0.55} \tag{49}$$

$$\hat{D}_{1,\,\mathrm{opt}} \cong 0.69\hat{M}^{0.101}\phi_1^{0.477} \tag{50}$$

$$\hat{H}_{0,\,\mathrm{opt}} \cong 1.11\hat{M}^{-0.202}\phi_1^{0.045} \tag{51}$$

such that the twice optimized overall flow resistance becomes:

$$\Delta\hat{P}_{1,\,\mathrm{mm}} \cong 3.66\hat{M}^{0.404}\phi_1^{-2.09} \tag{52}$$

The other features of the optimized assembly are

$$\left(\frac{D_1}{D_0}\right)_{\mathrm{opt}} \cong 1.02\left(\frac{\hat{M}}{4}\right)^{0.3}\phi_1^{-0.07} \tag{53}$$

$$\left(\frac{H_1}{L_1}\right)_{\mathrm{opt}} \cong 1.21\left(\frac{\hat{M}}{4}\right)^{-0.3}\phi_1^{0.07} \tag{54}$$

$$n_{1,\,\mathrm{opt}} \cong 2.01\left(\frac{\hat{M}}{4}\right)^{0.91}\phi_1^{-0.203} \tag{55}$$

These features agree qualitatively with the results determined in Eqs. (14) and (15) for the first construct with parallel-plate channels.

8. Conclusions

In this paper, we extended the constructal method to systems that are cooled volumetrically by tree networks of channels with fluid flow. The stream of coolant enters the volume through a single port and exits through another single port. Every point of the infinity of points of the heat generating volume is placed in contact with the coolant: the generated heat flows first by thermal diffusion through solid material, before it is collected by the first (smallest, elemental) stream of fluid.

The volume-constrained optimization of the paths for heat and fluid flow began with the smallest volume element, where a single duct collected the heat current integrated over the volume. It then continued toward larger volume scales in a stepwise sequence in which each larger volume is an assembly (a construct) of previously optimized smaller volumes. At the elemental level (Section 2), we found that the external shape of the volume element can be selected such that the global thermal resistance is minimum. Beginning with the first construct (Section 3), two geometric features can be optimized: the external shape of the construct, or the number of constituents ($n_1, n_2, \ldots$), and the ratio between the thickness of each new central duct and the thickness of its tributaries (D_1/D_0, $D_2/D_1, \ldots$). The optimal tapering of the profile of central ducts (Section 5) has only a minor effect on the global performance of the construct.

The existence of these geometric optima is in agree-

ment with the conclusions reached in the optimization of tree networks for pure heat conduction [1] and pure fluid flow [2]. Unlike in Refs. [1,2], the numbers of constituents do not decrease to 2 (dichotomy) as the order of the volume construct increases. The larger constructs become more slender: this means that if the largest construct must fit inside a volume with fixed external shape, then the constructal designs developed in this paper will not necessarily meet this objective. In such cases, the final stage of the optimization (the architecture of the largest volume) must be executed numerically.

Numerical progress can also be made on the sequence of constructal steps started in this paper. For example, the elemental system can be optimized numerically in the general case where the simplifying assumption $M > 4$ does not apply (see the end of Section 2). This unrestricted range of M values is important for the additional reason that, in it, the optimized elements and constructs are not necessarily slender and, consequently, they have a better chance of filling the total volume allocated to the system.

We end with a few clarifications in response to suggestions provided by the reviewers of the original manuscript. In this paper, the two-dimensional geometry was used for the sake of simplicity and clarity in presenting the method. The reason is that the new content of this paper — the tree structure that combines convection in the channels with conduction in the interstices — is more complicated than the constructal trees optimized in the past. For this first look at convective trees, we started in the simplest way, and, as we show in Section 7, we ended with an outline of how one may extend the constructal method to three-dimensional configurations.

The same approach was used in the reporting of the constructal method for simpler flows. For pure conduction, the first analyses done in two dimensions [1,3] were followed by an extension to three-dimensional heat-tree networks [11]. Similarly, the two-dimensional analyses of pure fluid flow between a volume and one point [3,12–14] were complemented but a construction in three dimensions [2,3]. The three-dimensional treatment of convective tree structures deserves to be considered in detail in future studies, perhaps by following the examples given in Refs. [2,11].

The tapering of parallel-plate channels (Fig. 4, bottom) is a feature required by the uniform distribution of flow rate through volumes of immediately smaller scale. It is true that the exact channel shape optimized in formulas such as Eq. (28) may be difficult to achieve in practice, especially the round shape near the narrow end. The important conclusion is that tapering is required by (i.e., goes hand-in-hand with) uniform volumetric bathing. It is also important that the exact tapering does not make a big difference in how the structure performs: note the similarities between Eqs. (31) and (32) and Eqs. (14) and (15).

We already commented on the route to larger scales, and why higher order constructs of the present type are not likely to fit in specified overall enclosures. The incorporation of higher order structures in the design (i.e., the increase in complexity) will make the system perform better [15]; however, the higher order structures may not fit in the given volume. It is important to keep in mind that all the length scales start from the elemental, and that the elemental scale is fixed. Trying to fit constructs of increasing higher order into a fixed volume would require a smaller and smaller elemental scale.

Examples of engineering systems, where the present convective trees may find applications, were discussed in Section 1. One specific example is the cooling of an enclosure filled with electronics, in which the coolant enters as a stream through one port, and exits through another. Stacks of printed circuits boards installed in this enclosure will play the role of first constructs, cf. Fig. 3. Another example was pointed out by one of the reviewers: the vascular anatomy of the chorioallantoic membrane, which is a respiratory organ in the embryonic chick.

Applications also exist in fuel cells and bio-reactors, which are systems where reactions occur volumetrically, and the reactions are sustained by streams that enter and exit through discrete points. For example, a bio-reactor produces enzymes by solid state fermentation. Due to metabolism, heat is generated and must be removed to keep the micro-organisms alive. One way too cool the solid mass is to insert cooling channels (cracks). The optimization opportunity arises from the need to allocate solid mass volume to the cooling network, in a constrained volume. The channels may also serve as conveyors of O_2 for respiration, if the process is aerobic.

A possible future application of the constructal method to the design of convective trees is the development of heat transfer models for living tissues. The way to begin was described by Huang et al. [16], who assumed two trees of convective tubes (one arterial, the other venous) almost superimposed, and in counterflow. This tree was embedded in a cube of solid tissue, which was covered by three-dimensional steady heat conduction. Tube diameters decreased by the same, assumed factor from one branching stage to the next. Dichotomy was also assumed: larger tubes were continued by two smaller tubes. This tree structure has features in common with the three-dimensional fluid tree deduced (optimized), based on the constructal method [2,3]. The main difference is that in the constructal tree the diameter reduction factor and the integer 2 (dichotomy, bifurcation, pairing) were optimization results, not assumptions. Huang et al.'s tree

expires in channels filling a "terminal subvolume": this subvolume is equivalent to the first construct defined in the present paper. Another major difference is that Huang et al. did not consider the fluid mechanics of the tree. They did not calculate and minimize the volume–point resistance to fluid flow.

Future work in bioheat transfer may reconsider Huang et al.'s model based on the constructal method. The smallest volume would be the elemental volume, and geometric optimization subject to volume and void constraints would be performed at every step. One difference, and a good question for future studies is the assumption of adiabatic contours (boundaries) for all the constructs described as building blocks in this paper. In Huang et al.'s model, heat was conducted across what would have been boundaries between constructs. In the case of pure heat conduction, we showed by numerical simulations that the presence of adiabatic internal boundaries between constructs has practically no effect on the global thermal resistance of the volume [15].

Acknowledgements

This work was supported by the National Science Foundation and Conselho Nacional de Desenvolvimento Cientifico e Tecnológico (CNPq), Brazil.

References

[1] A. Bejan, Constructal-theory network of conducting paths for cooling a heat generating volume, Int. J. Heat Mass Transfer 40 (1997) 799–816.
[2] A. Bejan, Constructal tree network for fluid flow between a finite-size volume and one source or sink, Rev. Gén. Thermique 36 (1997) 592–604.
[3] A. Bejan, Advanced Engineering Thermodynamics, 2nd ed., Wiley, New York, 1997.
[4] W. Aung (Ed.), Cooling Technology for Electronic Equipment, Hemisphere, New York, 1988.
[5] G.P. Peterson, A. Ortega, Thermal control of electronic equipment and devices, Advances in Heat Transfer 20 (1990) 181–314.
[6] S. Kakac, H. Yüncü, K. Hijikata (Eds.), Cooling of Electronic Systems, Kluwer Academic Publishers, Dordrecht, The Netherlands, 1994.
[7] R.C. Chu, R.E. Simons, Cooling technology for high performance computers: IBM sponsored university research, in: S. Kakac, H. Yüncü, K. Hijikata (Eds.), Cooling of Electronic Systems, Kluwer Academic Publishers, Dordrecht, The Netherlands, 1994, pp. 97–122.
[8] A. Bar-Cohen, W.M. Rohsenow, Thermally optimum spacing of vertical, natural convection cooled, parallel plates, J. Heat Transfer 106 (1984) 116–123.
[9] R.W. Knight, J.S. Goodling, D.J. Hall, Optimal thermal design of forced convection heat sinks — analytical, J. Electronic Packaging 113 (1991) 313–321.
[10] N.K. Anand, S.H. Kim, L.S. Fletcher, The effect of plate spacing on free convection between heated parallel plates, J. Heat Transfer 114 (1992) 515–518.
[11] G.A. Ledezma, A. Bejan, Constructal three-dimensional trees for conduction between a volume and one point, J. Heat Transfer 120 (1998) 977–984.
[12] A. Bejan, M.R. Errera, Deterministic tree networks for fluid flow: geometry for minimal flow resistance between a volume and one point, Fractals 5 (1997) 685–695.
[13] M.R. Errera, A. Bejan, Deterministic tree networks for river drainage basins, Fractals 6 (1998) 245–261.
[14] M.R. Errera, A. Bejan, Tree networks for flows in porous media, J. Porous Media 2 (1999) 1–18.
[15] A. Bejan, N. Dan, Two constructal routes to minimal heat flow resistance via greater internal complexity, J. Heat Transfer 121 (1999) 6–14.
[16] H.W. Huang, Z.P. Chen, R.B. Roemer, A counter current vascular network model of heat transfer in tissues, J. Biomechanical Engineering 118 (1996) 120–129.